# Spin-memory effect of $Tm^{2+}$ in cubic fields

T. Kohmoto
*Department of Physics, College of Liberal Arts and Sciences, Kyoto University, Sakyo-ku, Kyoto 606, Japan*

Y. Fukuda
*Department of Physics, College of Liberal Arts, Kobe University, Nada-ku, Kobe 657, Japan*

T. Hashi
*Department of Physics, Faculty of Science, Kyoto University, Sakyo-ku, Kyoto 606, Japan*
(Received 14 August 1990)

A theoretical investigation is made of the spin-memory effect of $Tm^{2+}$ in cubic fields which plays an important role in achieving the electron-spin polarization in the metastable state under optical pumping. The spin polarization, which is induced by the optical pumping to the absorption band and the spin-memory effect in the decay process from the band to the metastable state, is calculated by using the selection rules and the coupling coefficients for the cubic point group $O$. In the magnetic field, it is important that the selection rules and the coupling coefficients depend on the direction of the magnetic field and the value of the angular momentum $J$. From the results of the calculation, the observed spin polarizations can be explained if the decay has $T_1$ symmetry and the band has $G_{3/2}$ ($J=7/2$) character. The effect of hyperfine interactions is also discussed to explain the intensity ratio of the observed ESR signals.

## I. INTRODUCTION

The spin-memory effect in solids makes an important contribution to the creation of the electron-spin polarization in the excited state under optical pumping. In a previous paper,[1] which we refer to as paper I, we reported the optically detected low-field ESR in the metastable state of $Tm^{2+}$:$SrF_2$, where the population differences were created by optical pumping and spin-memory effect. This effect is a general phenomenon and has been observed in $Cr^{3+}$ in $Al_2O_3$,[2] in $Eu^{2+}$ in $CaF_2$,[3] in $M$-like center in CaO,[4] in $F$ center in alkali halides,[5–7] etc. In this paper we give the theoretical investigation of the spin-memory effect of $Tm^{2+}$ in cubic fields, which determines the population distribution among the magnetic sublevels in the metastable state.

As shown in the references of paper I, the optical and magnetic properties of the $Tm^{2+}$ ion in alkaline-earth fluoride hosts $CaF_2$, $SrF_2$, and $BaF_2$ have been extensively studied, and several interesting experiments have been performed on the $Tm^{2+}$ ion. The $Tm^{2+}$ ion is located in cubic fields ($O_h$) in these hosts. The energy-level diagram of $Tm^{2+}$ in $SrF_2$ is shown in Fig. 1. The lowest configuration $4f^{13}$ of the $Tm^{2+}$ ion is best pictured as a single hole in the filled $4f$ shell ($^2F$). The spin-orbit coupling splits the $^2F$ into the two states $^2F_{5/2}$ and $^2F_{7/2}$ separated by about 9000 $cm^{-1}$ with the latter lower. The cubic field splits these states further into doublets and quartets. Both of the ground ($^2F_{7/2}, E_{5/2}$) and the metastable ($^2F_{5/2}, E_{5/2}$) states are electronic doublets and can be described with the effective spin $\frac{1}{2}$. In the visible region this ion has a strong absorption band ascribed to the $4f^{12}5d$ configuration. The transition to the band shows large paramagnetic circular dichroism[1,8,9] and Faraday rotation.[1,10]

In paper I we reported the observation of the low-field ESR in the ground and the metastable states of

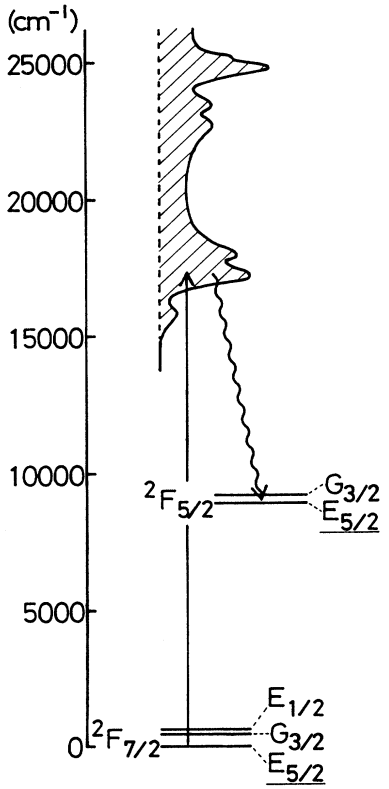


FIG. 1. Energy-level diagram of $Tm^{2+}$ in $SrF_2$.

 

$Tm^{2+}$:$SrF_2$. We achieved a very high detection sensitivity by using optical pumping and monitoring with cw lasers. The optical pumping with circularly polarized light created population differences in the ground state through preferential depopulation due to the circular dichroism of the optical transition. It also created population differences in the metastable state through preferential pumping to the absorption band and spin-memory effect in the decay process from the band to the metastable state. Faraday rotation due to these population differences were monitored by a polarimeter.

The spin-memory effect has been studied in $Tm^{2+}$:$CaF_2$ by Anderson and Sabisky[11] in high magnetic fields under optical pumping with a linearly polarized light incident perpendicular to the magnetic field. They observed that the spin polarization in the metastable state is induced in the same direction as that in the ground state. They showed that, when the magnetic field **H** is applied along the [001] axis, the experimental results could be explained by the decay of $T_1$ symmetry. However, no satisfactory interpretation was given to the results for $\mathbf{H}\|[111]$.

Our experiment in paper I was performed in low magnetic fields under optical pumping with circularly polarized light incident parallel to the magnetic field ($\mathbf{H}\|[111]$). It should be noted that the spin polarization created in the metastable state is in the opposite direction to that in the ground state, in contrast to the case of Anderson and Sabisky. Figure 2 schematically shows the spin polarizations established in the ground and metastable states by optical pumping from the ground state followed by spin-memory effect, where negative $g$ factor[12] is taken into account in the metastable state.

In this paper we discuss the spin-memory effect, which plays an important role in establishing the population distribution in the metastable state. We calculate the electron-spin polarization in the magnetic field along the [001] and [111] axes by using selection rules and coupling coefficients for the cubic point group $O$, which depend on the direction of the magnetic field and the value of the angular momentum $J$. We show that our experiment and that of Anderson and Sabisky can be explained on the same basis, and that the experimental results can be explained by the band of $G_{3/2}$ ($J=\frac{7}{2}$) character and the decay of $T_1$ symmetry.

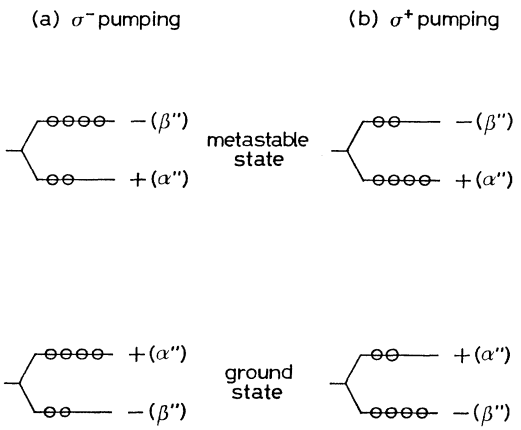


FIG. 2. Schematic spin polarization established in the ground and metastable states by the optical pumping and the spin-memory effect.

In Sec. II we show that the selection rules and the coupling coefficients for the cubic point group $O$ generally depend on the quantization axis and the $J$ value, and discuss the magnetic circular dichroism (MCD) of the optical transition. In Sec. III we calculate the electron-spin polarization induced in the metastable state by using results obtained in Sec. II and the Appendix. And we determine the characters of the electronic state and the decay responsible for the spin-memory effect. In Sec. IV we discuss the effect of hyperfine interaction to explain the population distribution among the sublevels of the metastable state.

## II. SELECTION RULES AND MCD OF THE OPTICAL TRANSITION

For the discussion of the spin-memory effect we need to derive the selection rules and the coupling coefficients for the cubic point group $O$. The transition probability between $\Gamma$ and $\Gamma''$ states for the transition of $\Gamma'$ symmetry is proportional to the square of the coupling coefficient

$$\langle \Gamma\gamma, \Gamma'\gamma' | \Gamma''\gamma'' \rangle , \tag{1}$$

where $\Gamma$ denotes one of the irreducible representation of the point group $O$ and $\gamma$ one of its bases.

In the point group $O$ the electronic configurations of a Kramers ion contain the irreducible representations $E_{1/2}$ (doublet), $E_{5/2}$ (doublet), and $G_{3/2}$ (quartet). For a rare earth ion in a $4f$ configuration the total angular momentum $J$ is a good quantum number, though it may not in the band. Therefore, it is convenient to consider the irreducible representations labeled by $J$. The reduction of the $(2J+1)$ states, $|J,M\rangle$, to the irreducible representations for half-integral values of $J$ (from $\frac{1}{2}$ to $\frac{9}{2}$) is given as follows:[13]

$$\begin{aligned}
&J=\tfrac{1}{2}\ , \quad E_{1/2}\ ;\\
&J=\tfrac{3}{2}\ , \quad G_{3/2}\ ;\\
&J=\tfrac{5}{2}\ , \quad E_{5/2}+G_{3/2}\ ;\\
&J=\tfrac{7}{2}\ , \quad E_{1/2}+E_{5/2}+G_{3/2}\ ;\\
&J=\tfrac{9}{2}\ , \quad E_{1/2}+2G_{3/2}\ .
\end{aligned} \tag{2}$$

The ground and metastable states of the $Tm^{2+}$ ion in the cubic fields correspond to $E_{5/2}$ ($J=\frac{7}{2}$) and $E_{5/2}$ ($J=\frac{5}{2}$), respectively.

The measurement of MCD on the band[8] have indicated that the transition can be described as purely electronic and governed by the selection rules for the electric-dipole operator in the cubic point group, and that the lowest-energy components of the band have mostly $G_{3/2}$ character. Therefore, we need not consider the value of $J$ other than $\frac{5}{2}$, $\frac{7}{2}$, and $\frac{9}{2}$ for the band because of the selection

rules for the electric-dipole transition from the ground state $E_{5/2}$ ($J=\frac{7}{2}$). The $4f^{12}5d$ configuration, which give rise to the band, contains 152 $G_{3/2}$ states,[8] and many $G_{3/2}$ ($J=\frac{5}{2},\frac{7}{2},\frac{9}{2}$) states originated from various spin-orbit-coupling states are possible in the band.

When the sublevels are degenerated, the general properties of the state are determined only by the irreducible representation $\Gamma$ ($E_{1/2}$, $E_{5/2}$, or $G_{3/2}$) independent of the selection of the bases $|\Gamma,\gamma\rangle$. However, we have to consider the spin-memory effect in the magnetic field, where the sublevels are not degenerated, so that the bases should be the eigenstates in the magnetic field. The bases expressed in terms of the eigenfunctions ($|J,M\rangle$) of a free ion are shown in Table I for $J=\frac{3}{2}$, $\frac{5}{2}$, and $\frac{7}{2}$ taking the [001] and [111] axes as the quantization axis $z$. The bases for the representations $E_{1/2}$, $E_{5/2}$, and $G_{3/2}$ are denoted as $(\alpha',\beta')$, $(\alpha'',\beta'')$, and $(\kappa,\lambda,\mu,\nu)$, respectively. They are the eigenstates in the magnetic field along the $z$ axis and are arranged so that the matrix element $\langle\Gamma,\gamma|\mathbf{J}_+|\Gamma,\gamma'\rangle$ has nonzero value between the upper base $\gamma$ and the lower base $\gamma'$. The derivation of the results in Table I is described in the Appendix. The bases are derived from the crystalline-field Hamiltonian $\mathcal{H}_c$ given by Eqs. (A1) and (A2), where the quantization axis is taken along the [001] and [111] axes. The bases in standard textbooks[14,15] are those for $\hat{\mathbf{z}}\|[001]$, while those for $\hat{\mathbf{z}}\|[111]$ are not found. In the ground and metastable states the plus- and minus-spin states are represented by $\alpha''$ and $\beta''$, where $\langle+|\mathbf{J}_+|-\rangle=\langle\alpha''|\mathbf{J}_+|\beta''\rangle\neq0$.

We are interested in the electron-spin polarization under the Zeeman interactions and neglect the hyperfine interactions in the present and the next sections. The effect of the hyperfine interactions, which will be discussed in Sec. IV, determines the population distribution among the magnetic sublevels of the metastable state but does not change the sign of the electron-spin polarization.

In Table I the bases for $J=\frac{9}{2}$ are not listed, though the electric-dipole transition is allowed between the $G_{3/2}$

TABLE I. Bases of the irreducible representations of the double cubic group for $J=\frac{3}{2}$, $\frac{5}{2}$, and $\frac{7}{2}$ taking the [001] and [111] axes as the quantization axis.

| | | $\hat{\mathbf{z}}\|[001]$ | $\hat{\mathbf{z}}\|[111]$ |
|---|---|---|---|
| $J=\frac{3}{2}$ | $\|G_{3/2},\kappa\rangle$ | $\|\frac{3}{2},+\frac{3}{2}\rangle$ | $\|\frac{3}{2},+\frac{3}{2}\rangle$ |
| | $\|G_{3/2},\lambda\rangle$ | $\|\frac{3}{2},+\frac{1}{2}\rangle$ | $\|\frac{3}{2},+\frac{1}{2}\rangle$ |
| | $\|G_{3/2},\mu\rangle$ | $\|\frac{3}{2},-\frac{1}{2}\rangle$ | $\|\frac{3}{2},-\frac{1}{2}\rangle$ |
| | $\|G_{3/2},\nu\rangle$ | $\|\frac{3}{2},-\frac{3}{2}\rangle$ | $\|\frac{3}{2},-\frac{3}{2}\rangle$ |
| $J=\frac{5}{2}$ | $\|E_{5/2},\alpha''\rangle$ | $\frac{1}{\sqrt{6}}\|\frac{5}{2},+\frac{5}{2}\rangle-\frac{\sqrt{5}}{\sqrt{6}}\|\frac{5}{2},-\frac{3}{2}\rangle$ | $-\frac{\sqrt{5}}{3}\|\frac{5}{2},+\frac{1}{2}\rangle+\frac{2}{3}\|\frac{5}{2},-\frac{5}{2}\rangle$ |
| | $\|E_{5/2},\beta''\rangle$ | $-\frac{\sqrt{5}}{\sqrt{6}}\|\frac{5}{2},+\frac{3}{2}\rangle+\frac{1}{\sqrt{6}}\|\frac{5}{2},-\frac{5}{2}\rangle$ | $\frac{2}{3}\|\frac{5}{2},+\frac{5}{2}\rangle+\frac{\sqrt{5}}{3}\|\frac{5}{2},-\frac{1}{2}\rangle$ |
| | $\|G_{3/2},\kappa\rangle$ | $-\frac{1}{\sqrt{6}}\|\frac{5}{2},+\frac{3}{2}\rangle-\frac{\sqrt{5}}{\sqrt{6}}\|\frac{5}{2},-\frac{5}{2}\rangle$ | $\|\frac{5}{2},-\frac{3}{2}\rangle$ |
| | $\|G_{3/2},\lambda\rangle$ | $\|\frac{5}{2},+\frac{1}{2}\rangle$ | $-\frac{2}{3}\|\frac{5}{2},+\frac{1}{2}\rangle-\frac{\sqrt{5}}{3}\|\frac{5}{2},-\frac{5}{2}\rangle$ |
| | $\|G_{3/2},\mu\rangle$ | $-\|\frac{5}{2},-\frac{1}{2}\rangle$ | $-\frac{\sqrt{5}}{3}\|\frac{5}{2},+\frac{5}{2}\rangle+\frac{2}{3}\|\frac{5}{2},-\frac{1}{2}\rangle$ |
| | $\|G_{3/2},\nu\rangle$ | $\frac{\sqrt{5}}{\sqrt{6}}\|\frac{5}{2},+\frac{5}{2}\rangle+\frac{1}{\sqrt{6}}\|\frac{5}{2},-\frac{3}{2}\rangle$ | $\|\frac{5}{2},+\frac{3}{2}\rangle$ |
| $J=\frac{7}{2}$ | $\|E_{1/2},\alpha'\rangle$ | $\frac{\sqrt{7}}{2\sqrt{3}}\|\frac{7}{2},+\frac{1}{2}\rangle+\frac{\sqrt{5}}{2\sqrt{3}}\|\frac{7}{2},-\frac{7}{2}\rangle$ | $\frac{\sqrt{5}}{3\sqrt{6}}\|\frac{7}{2},+\frac{7}{2}\rangle-\frac{\sqrt{7}}{3\sqrt{3}}\|\frac{7}{2},+\frac{1}{2}\rangle-\frac{\sqrt{35}}{3\sqrt{6}}\|\frac{7}{2},-\frac{5}{2}\rangle$ |
| | $\|E_{1/2},\beta'\rangle$ | $-\frac{\sqrt{5}}{2\sqrt{3}}\|\frac{7}{2},+\frac{7}{2}\rangle-\frac{\sqrt{7}}{2\sqrt{3}}\|\frac{7}{2},-\frac{1}{2}\rangle$ | $-\frac{\sqrt{35}}{3\sqrt{6}}\|\frac{7}{2},+\frac{5}{2}\rangle+\frac{\sqrt{7}}{3\sqrt{3}}\|\frac{7}{2},-\frac{1}{2}\rangle+\frac{\sqrt{5}}{3\sqrt{6}}\|\frac{7}{2},-\frac{7}{2}\rangle$ |
| | $\|E_{5/2},\alpha''\rangle$ | $\frac{\sqrt{3}}{2}\|\frac{7}{2},+\frac{5}{2}\rangle-\frac{1}{2}\|\frac{7}{2},-\frac{3}{2}\rangle$ | $\frac{\sqrt{7}}{3\sqrt{2}}\|\frac{7}{2},+\frac{7}{2}\rangle+\frac{\sqrt{5}}{3}\|\frac{7}{2},+\frac{1}{2}\rangle-\frac{1}{3\sqrt{2}}\|\frac{7}{2},-\frac{5}{2}\rangle$ |
| | $\|E_{5/2},\beta''\rangle$ | $\frac{1}{2}\|\frac{7}{2},+\frac{3}{2}\rangle+\frac{\sqrt{3}}{2}\|\frac{7}{2},-\frac{5}{2}\rangle$ | $\frac{1}{3\sqrt{2}}\|\frac{7}{2},+\frac{5}{2}\rangle+\frac{\sqrt{5}}{3}\|\frac{7}{2},-\frac{1}{2}\rangle-\frac{\sqrt{7}}{3\sqrt{2}}\|\frac{7}{2},-\frac{7}{2}\rangle$ |
| | $\|G_{3/2},\kappa\rangle$ | $\frac{\sqrt{3}}{2}\|\frac{7}{2},+\frac{3}{2}\rangle+\frac{1}{2}\|\frac{7}{2},-\frac{5}{2}\rangle$ | $-\|\frac{7}{2},+\frac{3}{2}\rangle$ |
| | $\|G_{3/2},\lambda\rangle$ | $-\frac{\sqrt{5}}{2\sqrt{3}}\|\frac{7}{2},+\frac{1}{2}\rangle+\frac{\sqrt{7}}{2\sqrt{3}}\|\frac{7}{2},-\frac{7}{2}\rangle$ | $-\frac{\sqrt{14}}{3\sqrt{3}}\|\frac{7}{2},+\frac{7}{2}\rangle+\frac{\sqrt{5}}{3\sqrt{3}}\|\frac{7}{2},+\frac{1}{2}\rangle-\frac{2\sqrt{2}}{3\sqrt{3}}\|\frac{7}{2},-\frac{5}{2}\rangle$ |
| | $\|G_{3/2},\mu\rangle$ | $\frac{\sqrt{7}}{2\sqrt{3}}\|\frac{7}{2},+\frac{7}{2}\rangle-\frac{\sqrt{5}}{2\sqrt{3}}\|\frac{7}{2},-\frac{1}{2}\rangle$ | $\frac{2\sqrt{2}}{3\sqrt{3}}\|\frac{7}{2},+\frac{5}{2}\rangle+\frac{\sqrt{5}}{3\sqrt{3}}\|\frac{7}{2},-\frac{1}{2}\rangle+\frac{\sqrt{14}}{3\sqrt{3}}\|\frac{7}{2},-\frac{7}{2}\rangle$ |
| | $\|G_{3/2},\nu\rangle$ | $\frac{1}{2}\|\frac{7}{2},+\frac{5}{2}\rangle+\frac{\sqrt{3}}{2}\|\frac{7}{2},-\frac{3}{2}\rangle$ | $-\|\frac{7}{2},-\frac{3}{2}\rangle$ |

($J=\frac{9}{2}$) state and the ground state. In the case of $J=\frac{9}{2}$, there is a complexity arising from the fact that we have two $G_{3/2}$ states; the eigenfunctions depend on an unknown factor $B_4/B_6$ in the band,[16] where $B_4$ and $B_6$ are the coefficients of the fourth and sixth degree operator of the crystalline-field Hamiltonian $\mathcal{H}_c$ [Eqs. (A1) and (A2) in the Appendix]. Therefore, it is not easy to discuss the $G_{3/2}$ ($J=\frac{9}{2}$) state in the band. Besides, the $G_{3/2}$ ($J=\frac{9}{2}$) state would not make a dominant contribution to the spin polarization in the metastable state, as will be mentioned in Sec. III.

In this paper our discussion on the $G_{3/2}$ state is restricted to $J=\frac{5}{2}$ and $\frac{7}{2}$. We also discuss the $G_{3/2}$ ($J=\frac{3}{2}$) state for comparison, although the transition between the state and the ground state is forbidden.

In this section we pay attention to the optical transition and show the selection rules and the coupling coefficients for the transition of $T_1$ symmetry. The coupling coefficients for general symmetries are given in the Appendix. The electric-dipole transition is allowed from a $E_{5/2}$ state to $E_{5/2}$ and $G_{3/2}$ states, but forbidden to $E_{1/2}$ states ($E_{5/2}\times T_1=E_{5/2}+G_{3/2}$). Table II shows the selection rules for the electric-dipole transition ($T_1$) between $|E_{5/2},\gamma\rangle$ and $|\Gamma'',\gamma''\rangle$ levels and the normalized coupling coefficients

$$\langle E_{5/2}\gamma, T_1\gamma'|\Gamma''\gamma''\rangle\ , \tag{3}$$

where

$$\gamma=\alpha'',\beta''\ ,$$

$$\gamma'=+1\ (\sigma^+),\ 0\ (\pi),\ -1\ (\sigma^-)\ ,$$

$$\Gamma''=E_{1/2},E_{5/2},G_{3/2},$$

and

$$\gamma''=\alpha',\beta'\ (\Gamma''=E_{1/2}),\quad \alpha'',\beta''\ (\Gamma''=E_{5/2})\ ,$$

$$\kappa,\lambda,\mu,\nu\ (\Gamma''=G_{3/2})\ .$$

The derivation of the results in Table II is also described in the Appendix. We obtained the coupling coefficients from the bases in Table I and the Clebsch-Gordan coefficients. The Clebsch-Gordan coefficients are the coupling coefficients for the rotation group, and the coupling coefficients, whose definition is given by Eq. (A3), may be called the generalized Clebsch-Gordan coefficients.

In the case of the magnetic field along the [001] axis, the selection rules and the coupling coefficients [Table II(a)] between $E_{5/2}$ and $\Gamma''$ ($E_{1/2}$, $E_{5/2}$, or $G_{3/2}$) states do not depend on the $J$ value; calculations show that these are the same for $J=\frac{3}{2}$, $\frac{5}{2}$, and $\frac{7}{2}$. The coupling coefficients between $G_{3/2}$ states depend on the $J$ value, though not shown in Table II. In the case of the magnetic field along the [111] axis, on the other hand, the coupling coefficients between $E_{5/2}$ and $G_{3/2}$ states are different for different $J$ values of the $G_{3/2}$ state as shown in Table II(b), although they do not depend on the $J$ value of the $E_{5/2}$ state ($J=\frac{5}{2}$ and $\frac{7}{2}$). Those between $E_{5/2}$ states are the same as in Table II(a) and independent of the $J$ value. Thus, the selection rules and the coupling coefficients generally depend on the quantization axis and the $J$ value. This result arises from the fact that the selection of the bases depends on the direction of the magnetic field and the $J$ value even if the states belong to the same irreducible representation. In this paper we point out the importance of the quantization-axis and the $J$-value dependences of the selection rules and the coupling coefficients.

Before discussing the spin-memory effect we consider the MCD of the transition from the ground state ($E_{5/2}$) to the band. The electric-dipole transition is allowed to $E_{5/2}$ and $G_{3/2}$ states in the band. In high magnetic fields and low temperatures ($\mu_B H/kT\gg 1$), most of the ions are in the ground-state sublevel $|E_{5/2},\beta''\rangle$. Table II shows that, for the transitions from the $|E_{5/2},\beta''\rangle$ state to the $G_{3/2}$ states in the band, the ratio of the absorption coefficients $\alpha^+:\alpha^-$ for the $\sigma^+$ and $\sigma^-$ circularly polarized lights is always 1:3 independent of the field direction and the $J$ value. For the transitions to the $E_{5/2}$ states in the band, only the $\sigma^+$ polarized light is absorbed. Therefore the measure of MCD

$$D=\frac{\alpha^+-\alpha^-}{\alpha^++\alpha^-} \tag{4}$$

should be $-0.5$ for the transitions to the $G_{3/2}$ states and $+1$ for the $E_{5/2}$ states independent of the field direction and the $J$ value.

The observed MCD spectrum[1,17] shows that the value of $D$ in Eq. (4) is negative in the strong-absorption part of the band between 5300 and 6000 Å. This indicates that the band in this region has mostly $G_{3/2}$ character. In fact, the value $-0.21$ ($-0.37$) of $D$ at 5800 Å (6000 Å) suggests that the $G_{3/2}$ and $E_{5/2}$ parts of the band at this wavelength are 81 and 19% (91 and 9%), respectively. In the next section we assume that the optically pumped state in the band has a $G_{3/2}$ character. The same discussion is also valid for $Tm^{2+}$:$CaF_2$ except for the shift of the absorption spectrum.

## III. SPIN POLARIZATION IN THE METASTABLE STATE DUE TO THE SPIN-MEMORY EFFECT

In this section we calculate the electron-spin polarization in the metastable state considering the spin-memory effect in the spontaneous transition (decay) from the band to the metastable state. We assume that the spin polarization is created by the preferential pumping from the ground state $E_{5/2}$ ($J=\frac{7}{2}$) to a $G_{3/2}$ state in the band followed by a decay from the $G_{3/2}$ state to the metastable state $E_{5/2}$ ($J=\frac{5}{2}$) without any relaxation among the sublevels of the $G_{3/2}$ state.

According to the group theory there are three possible symmetries $E$, $T_1$, and $T_2$ for the decay from a $G_{3/2}$ state to a $E_{5/2}$ state ($G_{3/2}\times E_{5/2}=E+T_1+T_2$). The coupling coefficients given in Table II can be used for the decay of $T_1$ symmetry. We also calculated the coupling coefficients for $E$ and $T_2$ symmetries as shown in Table V (Appendix). From these coupling coefficients we obtained the expected values of the spin polarization in the metastable state

$$P^* = \frac{n_+^* - n_-^*}{n_+^* + n_-^*} , \tag{5}$$

where $n_\pm^*$ represents the population in the $\pm$ spin level of the metastable state. We first calculated the relative pumping rate into the sublevels ($\kappa$, $\lambda$, $\mu$, and $\nu$) of the $G_{3/2}$ state in the band under the optical pumping from the ground state by using the coupling coefficients for the electric-dipole transition in Table II. Then, we calculated the population distribution in the metastable state achieved by the spontaneous transition from the selectively populated $G_{3/2}$ sublevels to the metastable state.

TABLE II. Selection rules for the electric-dipole transition ($T_1$) and normalized coupling coefficients $\langle E_{5/2}\gamma, T_1\gamma' | \Gamma''\gamma'' \rangle$ for the cubic point group $O$. The quantization axis is taken (a) along the [001] axis and (b) along the [111] axis. The selection rules and the coupling coefficients for $\Gamma'' = E_{1/2}$ and $E_{5/2}$ in (b) are the same as in (a) and independent of the $J$ value.

(a) $\hat{\mathbf{z}} \| [001]$

| | | $E_{1/2}$ | | $E_{5/2}$ | |
|---|---|---|---|---|---|
| | | $\alpha'$ | $\beta'$ | $\alpha''$ | $\beta''$ |
| $E_{5/2}$ | $\alpha''$ | 0 | 0 | $\pi\left(\frac{1}{\sqrt{3}}\right)$ | $\sigma^-\left(\frac{\sqrt{2}}{\sqrt{3}}\right)$ |
| | $\beta''$ | 0 | 0 | $\sigma^+\left(-\frac{\sqrt{2}}{\sqrt{3}}\right)$ | $\pi\left(-\frac{1}{\sqrt{3}}\right)$ |

$G_{3/2}$ $(J = \frac{3}{2}, \frac{5}{2}, \frac{7}{2})$

| | | $\kappa$ | $\lambda$ | $\mu$ | $\nu$ |
|---|---|---|---|---|---|
| $E_{5/2}$ | $\alpha''$ | $\sigma^-\left(\frac{1}{\sqrt{3}}\right)$ | 0 | $\sigma^+(-1)$ | $\pi\left(\frac{\sqrt{2}}{\sqrt{3}}\right)$ |
| | $\beta''$ | $\pi\left(\frac{\sqrt{2}}{\sqrt{3}}\right)$ | $\sigma^-(-1)$ | 0 | $\sigma^+\left(\frac{1}{\sqrt{3}}\right)$ |

(b) $\hat{\mathbf{z}} \| [111]$

$G_{3/2}$ $(J = \frac{3}{2})$

| | | $\kappa_{3/2}$ | $\lambda_{3/2}$ | $\mu_{3/2}$ | $\nu_{3/2}$ |
|---|---|---|---|---|---|
| $E_{5/2}$ | $\alpha''$ | $\sigma^+\left(-\frac{1}{3}\right)$ | $\pi\left(\frac{\sqrt{2}}{\sqrt{3}}\right)$ | $\sigma^-\left(-\frac{1}{\sqrt{3}}\right)$ | $\sigma^+\left(\frac{2\sqrt{2}}{3}\right)$ |
| | $\beta''$ | $\sigma^-\left(\frac{2\sqrt{2}}{3}\right)$ | $\sigma^+\left(\frac{1}{\sqrt{3}}\right)$ | $\pi\left(-\frac{\sqrt{2}}{\sqrt{3}}\right)$ | $\sigma^-\left(\frac{1}{3}\right)$ |

$G_{3/2}$ $(J = \frac{5}{2})$

| | | $\kappa_{5/2}$ | $\lambda_{5/2}$ | $\mu_{5/2}$ | $\nu_{5/2}$ |
|---|---|---|---|---|---|
| $E_{5/2}$ | $\alpha''$ | $\sigma^+\left(-\frac{1}{\sqrt{3}}\right)$ | $\pi\left(\frac{\sqrt{2}}{\sqrt{3}}\right)$ | $\sigma^-\left(-\frac{1}{\sqrt{3}}\right)$ | $\sigma^+\left(\frac{\sqrt{2}}{\sqrt{3}}\right)$ |
| | $\beta''$ | $\sigma^-\left(\frac{\sqrt{2}}{\sqrt{3}}\right)$ | $\sigma^+\left(\frac{1}{\sqrt{3}}\right)$ | $\pi\left(-\frac{\sqrt{2}}{\sqrt{3}}\right)$ | $\sigma^-\left(\frac{1}{\sqrt{3}}\right)$ |

$G_{3/2}$ $(J = \frac{7}{2})$

| | | $\kappa_{7/2}$ | $\lambda_{7/2}$ | $\mu_{7/2}$ | $\nu_{7/2}$ |
|---|---|---|---|---|---|
| $E_{5/2}$ | $\alpha''$ | $\sigma^+\left(-\frac{5}{3\sqrt{3}}\right)$ | $\pi\left(\frac{\sqrt{2}}{\sqrt{3}}\right)$ | $\sigma^-\left(-\frac{1}{\sqrt{3}}\right)$ | $\sigma^+\left(\frac{\sqrt{2}}{3\sqrt{3}}\right)$ |
| | $\beta''$ | $\sigma^-\left(\frac{\sqrt{2}}{3\sqrt{3}}\right)$ | $\sigma^+\left(\frac{1}{\sqrt{3}}\right)$ | $\pi\left(-\frac{\sqrt{2}}{\sqrt{3}}\right)$ | $\sigma^-\left(\frac{5}{3\sqrt{3}}\right)$ |

The spin-memory effect due to the three possible symmetries of the spontaneous transition was examined by using the coupling coefficients in Table V.

Table III shows the calculated electron-spin polarization in the magnetic field along the [001] axis and the [111] axis for different $J$ values of the $G_{3/2}$ state in the band. We calculated the spin polarization in two cases; (a) in low magnetic fields under an optical pumping with circularly polarized light incident parallel to the magnetic field and (b) in high magnetic fields under an optical pumping with linearly polarized light incident perpendicular to the magnetic field. Our experiment corresponds to case (a), and that of Anderson and Sabisky to case (b). Weak and strong pumpings in case (a) mean that the optical pumping time is much longer and shorter than the spin-lattice-relaxation time in the ground state. The calculated values in case (a) are obtained by assuming that the population ratio in the ground state $n_+ : n_-$ is 1:1 for weak $\sigma^-$ pumping and 3:1 for strong $\sigma^-$ pumping, where $n_\pm$ represents the population in the $\pm$ spin level of the ground state. The population ratio for the strong pumping is the inverse ratio of the pumping rates from the sublevels expected from the electric-dipole transition to the $G_{3/2}$ state in the band. For $\sigma^+$ pumping the absolute value of the spin polarization is the same with the case of the $\sigma^-$ pumping, but the sign is reversed. The calculated values in case (b) are obtained by assuming that only the minus-spin level is populated in the ground state ($\mu_B H/kT \gg 1$, weak pumping). The spin polarization $P^*$ depends on the field direction and the $J$ value, while the MCD is independent of them as mentioned in Sec. II. These dependences arise from those of the spin-memory effect in the decay process.

In our experiment in paper I the spin polarization $P^*$ under the $\sigma^-$ pumping in low magnetic fields along the [111] axis was negative both for the weak and strong pumpings (Fig. 2). Table III(a) shows that our result can be explained only by the decay of $T_1$ symmetry for any of the $J$ values for the $G_{3/2}$ state. Other symmetries give positive or nearly zero polarizations. The calculated spin polarizations in Table III(b) are those which should be compared with the experimental results of Anderson and Sabisky.[11] For symmetry $T_1$, Table III(b) shows that the spin polarization is always negative, and that, for $\mathbf{H}\|[001]$, the polarization $(-0.67)$ for the $\sigma$ pumping is twice as large as that $(-0.33)$ for the $\pi$ pumping. These are just observed by Anderson and Sabisky.

On the other hand, for $\mathbf{H}\|[111]$, they predicted that the spin-memory effect should be less sensitive to the polarization of the pumping light. However, this prediction was in contradiction to their observation; similar light-polarization dependence was observed for all directions of the magnetic field. We suppose that they were unconcerned with the importance of the $J$ dependence, and that their prediction was based on the coupling coefficients for the $G_{3/2}$ ($J=\frac{3}{2}$) state,[9] for which Table III(b) gives the polarizations $-0.37(\sigma)$ and $-0.33(\pi)$. If so, this is not suitable because the electric-dipole transition to the states with $J=\frac{3}{2}$ is forbidden from the ground state ($J=\frac{7}{2}$).

Now we should consider the $G_{3/2}$ ($J=\frac{5}{2}$) and $G_{3/2}$ ($J=\frac{7}{2}$) states in the band with the decay of $T_1$ symmetry. The $G_{3/2}$ ($J=\frac{5}{2}$) state does not explain their observation because no polarization is expected for the $\sigma$ pumping. If the $G_{3/2}$ ($J=\frac{7}{2}$) state in the band is assumed to be responsible for the spin-memory effect, their experimental results can be explained; Table III(b) ($\mathbf{H}\|[111]$) gives the polarizations $-0.46(\sigma)$ and $-0.33(\pi)$ consistent with their observation. To the authors' knowledge, the importance of the $J$ dependence of the coupling coefficients has not been recognized so far.

It is noted that $T_1$ is the symmetry of the electric-dipole operator and this implies that the decay may be a radiative one. In fact, one phonon process is impossible because the energy difference ($\sim 7000\ \mathrm{cm}^{-1}$) between the lowest part of the band and the metastable state is much

TABLE III. Calculated electron-spin polarization $P^*$ in the metastable state induced by the optical pumping and the spin-memory effect. Three symmetries ($E$, $T_1$, and $T_2$) are possible for the decay from $G_{3/2}$ states in the band to the metastable state $E_{5/2}$.

| | Symmetry of the decay | $\mathbf{H}\|[001]$ $G_{3/2}$ ($J=\frac{3}{2},\frac{5}{2},\frac{7}{2}$) | $G_{3/2}$ ($J=\frac{3}{2}$) | $\mathbf{H}\|[111]$ $G_{3/2}$ ($J=\frac{5}{2}$) | $G_{3/2}$ ($J=\frac{7}{2}$) |
|---|---|---|---|---|---|
| | | (a) Parallel pumping in low fields | | | |
| Weak | $E$ | 0.50 | 0.06 | 0.06 | 0.75 |
| $\sigma^-$ pumping | $T_1$ | −0.83 | −0.54 | −0.17 | −0.63 |
| | $T_2$ | 0.50 | 0.50 | 0.13 | 0.13 |
| Strong | $E$ | 0.00 | 0.37 | 0.37 | 0.83 |
| $\sigma^-$ pumping | $T_1$ | −0.67 | −0.47 | −0.22 | −0.53 |
| | $T_2$ | 0.17 | 0.22 | −0.02 | −0.02 |
| | | (b) Perpendicular pumping in high fields | | | |
| $\sigma$ pumping | $E$ | 1.00 | −0.44 | −0.44 | 0.25 |
| | $T_1$ | −0.67 | −0.37 | 0.00 | −0.46 |
| | $T_2$ | 0.00 | 0.67 | 0.30 | 0.30 |
| $\pi$ pumping | $E$ | −1.00 | 1.00 | 1.00 | 1.00 |
| | $T_1$ | −0.33 | −0.33 | −0.33 | −0.33 |
| | $T_2$ | 1.00 | −0.33 | −0.33 | −0.33 |

larger than the Debye temperature of the host crystal ($\sim$500 K). The rate of multiphonon process rapidly decreases as the energy difference becomes large,[18,19] and then the higher-order processes will not be efficient in the short lifetime of the band, which is of the order of $10^{-8}$ sec from our measurement. As described in Sec. II we did not consider the $G_{3/2}$ ($J=\frac{9}{2}$) state in the band, though the state is possible to be pumped from the ground state. However, the transition from the state with $J=\frac{9}{2}$ in the band to the metastable state ($J=\frac{5}{2}$) is forbidden if the decay is radiative, and the other higher-order processes for the transition of $\Delta J=2$ with the large energy difference will not be efficient in the short lifetime. Therefore, we consider that the $G_{3/2}$ ($J=\frac{9}{2}$) state does not make a dominant contribution to the spin-memory effect.

From the above argument we conclude that the decay of $T_1$ symmetry explains the observed signs of the spin polarization in the metastable state, and that the dominant contribution to the spin-memory effect comes from the $G_{3/2}$ ($J=\frac{7}{2}$) state in the band. In our low-field experiment, the spin polarization achieved in the metastable state was in the opposite direction to that in the ground state. This is in contrast to the high-field experiment of Anderson and Sabisky, where the spin polarization was preserved. The difference arises from the excitation process to the band. As to the spin-memory effect from the band to the metastable state, our experiment and that of Anderson and Sabisky can be explained on the same basis, i.e., the selection rules and the coupling coefficients for the cubic point group $O$.

## IV. EFFECT OF HYPERFINE INTERACTIONS

In the preceding sections we neglected the nuclear spin and discussed only the electron-spin polarization. To explain the observed ESR signals, we have to consider the nuclear spin and the hyperfine interactions.

The hyperfine structure arises from the interaction

$$\mathcal{H}_J=g_J\mu_B\mathbf{J}\cdot\mathbf{H}+a_J\mathbf{J}\cdot\mathbf{I}\ , \tag{6}$$

where $g_J$ and $a_J$ are the Landé $g$ factor and the hyperfine constant in the spin-orbit coupling state of a free ion. The Hamiltonian (6) is regarded as a perturbation to the doublets or quartets ($E_{1/2}$, $E_{5/2}$, or $G_{3/2}$) in the crystalline field, whose eigenfunctions are given in Table I. The hyperfine interaction splits a doublet into four levels and a quartet into eight levels because the nuclear spin $I$ of $^{169}Tm$ is $\frac{1}{2}$.

For high magnetic fields the electron and the nucleus are decoupled ($g_J\mu_BH\gg a_J$), so that the ESR signals observed by Anderson and Sabisky[11] directly reflect the electron-spin polarization discussed in Sec. III. In this section we consider the hyperfine interactions in the ground state, in the metastable state, and in the band. We calculate the population distribution created by the spin-memory effect among the sublevels of the metastable state in the low magnetic fields, and try to explain the intensity ratio of the observed ESR signals.

Before discussing the effect of the hyperfine interactions, we consider what fraction of the pumped ions decay to the metastable state. We observed fluorescence (1.1 $\mu$m of wavelength and $\sim10^{-2}$ sec of lifetime at liquid helium temperatures) from the metastable state of $Tm^{2+}$:$SrF_2$ (0.02% $Tm^{2+}$) under the optical pumping to the band with a cw dye laser. We analyzed power dependence of the transient behavior and steady-state intensity of the fluorescence by using rate equations, and obtained a result that the value of the fraction $\eta$ is about 0.1. This value is nearly equal to the observed quantum efficiency of the fluorescence 0.08 in $Tm^{2+}$:$CaF_2$.[20] The small value of $\eta$ indicates that most of the pumped ions return to the ground state without populating in the metastable state. In fact, when we made an optical excitation to the band of $Tm^{2+}$:$SrF_2$ with nanosecond laser pulses, emission from the band to the ground state whose lifetime is $\sim10^{-8}$ sec was observed in a broad wavelength region (in the visible and infrared regions). Therefore, the ions which decay from the metastable state have little effect on the population distribution in the ground state, and the population distribution in the ground state is determined independent of that in the metastable state.

The electron and nuclear polarizations in the ground state has been discussed by Grant *et al.*[21] for $Tm^{2+}$:$CaF_2$. They showed that the population distribution in the ground state is well understood by assuming complete nuclear spin memory and randomized electron spin return in the optical pumping cycle. From this assumption we get the population distribution in the ground state

$$n_1:n_2:n_3:n_4=u_+^2:u_+u_-:u_-^2:u_+u_-\ , \tag{7}$$

where $n_i$ represents population in the $i$th sublevel (see Fig. 1 in paper I) and $u_\pm$ represents pumping rate from $\pm$ electron-spin level. In the derivation of Eq. (7) we neglected the spin-lattice relaxation in the ground state, which corresponds to the strong-pumping case. The distribution in Eq. (7) does not depend on the magnitude of the magnetic field. This population distribution becomes

$$n_1:n_2:n_3:n_4=0.16:0.24:0.36:0.24\ , \tag{8}$$

when we pump $Tm^{2+}$ ions in $SrF_2$ with $\sigma^-$ polarization at 5800 Å ($u_+:u_-\simeq2:3$). This distribution explains the intensities of the observed ESR signals in the ground state of $Tm^{2+}$:$SrF_2$ (paper I). Therefore, we start our discussion from the population distribution in Eq. (8) in the ground state.

The hyperfine structures are known in the ground and metastable states as described in the previous papers.[1,12] Although we do not have any information on the hyperfine interaction in the band, it is instructive to examine the two extreme cases; the electron and the nucleus in the band are

(A) completely decoupled ($g_J\mu_BH\gg a_J$)

and

(B) completely coupled ($a_J\gg g_J\mu_BH$) .

As discussed in Sec. III the dominant contribution to

the spin-memory effect comes from the band of $G_{3/2}$ ($J=\frac{7}{2}$) character and the decay of $T_1$ symmetry. Therefore, we use these electronic character and symmetry in the following and neglect the interaction between the $G_{3/2}$ ($J=\frac{7}{2}$) state and other states in the band. The population distribution $n_1^*:n_2^*:n_3^*:n_4^*$ in the metastable state is calculated in the two cases (A) and (B) under these assumptions. Since our ESR experiment was performed in the magnetic field along the [111] axis, we take the quantization axis $z$ along the [111] axis. The electron-spin polarization $P^*$ and the intensity ratio of the ESR signals $I_{12}^*:I_{23}^*$ are obtained from the distribution as

$$P^*=\frac{n_+^*-n_-^*}{n_+^*+n_-^*}=\frac{n_3^*-n_1^*+(a^{*2}-b^{*2})(n_4^*-n_2^*)}{n_1^*+n_2^*+n_3^*+n_4^*}\ ,$$
$$I_{12}^*:I_{23}^*=b^{*2}(n_1^*-n_2^*):a^{*2}(n_2^*-n_3^*)\ , \tag{9}$$

where the definitions of $n_i^*$, $I_{ij}^*$, $a^*$, and $b^*$ are the same as in paper I.

In case (A) the eigenfunctions of a $G_{3/2}$ ($J=\frac{7}{2}$) state are given by

$$|\kappa_{7/2}\rangle|I_z\rangle\ ,\quad |\lambda_{7/2}\rangle|I_z\rangle\ ,\quad |\mu_{7/2}\rangle|I_z\rangle\ ,$$

and (10)

$$|\nu_{7/2}\rangle|I_z\rangle\ ,$$

where $|\kappa_{7/2}\rangle$, $|\lambda_{7/2}\rangle$, $|\mu_{7/2}\rangle$, and $|\nu_{7/2}\rangle$ are the electronic eigenfunctions of the $G_{3/2}$ ($J=\frac{7}{2}$) state given in Table I ($\hat{\mathbf{z}}\|[111]$) and are eigenfunctions of the first (Zeeman) term in the Hamiltonian (6) in the magnetic field, and $|I_z\rangle$ represents the nuclear eigenfunction $|I_z=\pm\frac{1}{2}\rangle$. From eigenfunctions (10) and the eigenfunctions of the $E_{5/2}$ state given by Eq. (3) of paper I ($|+\pm\rangle$ and $|-\pm\rangle$ should be replaced by $|\alpha''\rangle|\pm\frac{1}{2}\rangle$ and $|\beta''\rangle|\pm\frac{1}{2}\rangle$ for the discussion here), we derived the selection rules and the coupling coefficients for $T_1$ symmetry between the four levels ($E_{5/2}$) and eight levels ($G_{3/2}$). Then we obtained the population distribution in the metastable state induced by the preferential pumping and the spin-memory effect after a procedure similar to that described in Sec. III. The $\sigma^-$ pumping from the ground state at 5800 Å and 200 Oe ($a^{*2}=0.665$ and $b^{*2}=0.335$), for example, followed by the decay of $T_1$ symmetry results in the distribution

$$n_1^*:n_2^*:n_3^*:n_4^*=0.32:0.35:0.12:0.21\ . \tag{11}$$

If this distribution is achieved in the metastable state, the electron-spin polarization and the intensity ratio of the ESR signals in Eqs. (9) are given by

$$P^*=-0.24\ ,\quad I_{12}^*:I_{23}^*=-0.06:1.00\ . \tag{12}$$

This calculated intensity ratio is quite different from the observed one in paper I. The intensities $I_{12}^*$ and $I_{23}^*$ observed at the same magnetic field are nearly equal.

In case (B) the eigenfunctions are given by linear combinations of those in case (A). We calculated the eigenfunctions of the Hamiltonian (6) taking the Zeeman term as a perturbation. At zero magnetic field, the energy levels of a $G_{3/2}$ ($J=\frac{7}{2}$) state are reduced to a doublet at $(\frac{7}{4})a_J$ and two triplets at $(\frac{1}{12})a_J$ and $(-\frac{5}{4})a_J$. From the selection rules and the coupling coefficients calculated from the eigenfunctions, we obtained the population distribution in the metastable state

$$n_1^*:n_2^*:n_3^*:n_4^*=0.31:0.27:0.23:0.19 \tag{13}$$

under the same conditions as in case (A). In the present case the electron-spin polarization and the intensity ratio in Eqs. (9) are given by

$$P^*=-0.11\ ,\quad I_{12}^*:I_{23}^*=0.67:1.00\ . \tag{14}$$

This intensity ratio agrees with the observed one, although the agreement is not complete.

In both cases the hyperfine interactions reduce the electron-spin polarization, but the sign of the polarization is not changed. The observed ESR signals in low-magnetic fields (~200 Oe) are understood if the electron and the nucleus are coupled rather than decoupled in the band. The difference between the calculation and the observation seems to come from the fact that we examined only the dominant contribution in the extreme cases; the spin-memory effects due to the band of $G_{3/2}$ ($J=\frac{7}{2}$) character and the decay of $T_1$ symmetry in the completely coupled and decoupled cases. However, it is difficult to estimate the corrections for the above calculation.

## V. SUMMARY

The spin-memory effect of $Tm^{2+}$ in cubic fields was investigated theoretically. We obtained the selection rules and the coupling coefficients for the cubic point group $O$, and calculated the electron-spin polarization in the metastable state achieved by the optical pumping and the spin-memory effect. It was recognized that dependences of the coupling coefficients on the quantization axis and the $J$ value are very important for the analysis of the population distribution in the magnetic field. The observed spin polarizations in our low-field experiment and the high-field experiment of Anderson and Sabisky were understood on the same basis. The dominant contribution to the spin-memory effect comes from the band of $G_{3/2}$ ($J=\frac{7}{2}$) character and the decay of $T_1$ symmetry. In low-magnetic fields as in our experiment the electron and the nucleus are coupled through the hyperfine interaction rather than decoupled in the band.

## ACKNOWLEDGMENTS

We would like to thank Professor T. Murao for helpful discussion on the selection rules.

## APPENDIX: COUPLING COEFFICIENTS FOR THE CUBIC POINT GROUP $O$

The selection rules and the transition probabilities used in Secs. II and III are obtained from the coupling coefficients of the irreducible representations in the cubic field. Here, we derive the eigenfunctions of the crystalline-field Hamiltonian, and then obtain the cou-

TABLE IV. Bases of the irreducible representations $E$, $T_1$ and $T_2$ of the cubic group for $J=1$ and 2 taking the [001] and [111] axes as the quantization axis.

| | | $\hat{z}\parallel[001]$ | $\hat{z}\parallel[111]$ |
|---|---|---|---|
| $J=1$ | $\lvert T_1,+1\rangle$ | $\lvert 1,+1\rangle$ | $\lvert 1,+1\rangle$ |
| | $\lvert T_1,0\rangle$ | $\lvert 1,0\rangle$ | $\lvert 1,0\rangle$ |
| | $\lvert T_1,-1\rangle$ | $\lvert 1,-1\rangle$ | $\lvert 1,-1\rangle$ |
| $J=2$ | $\lvert E,\theta\rangle$ | $\lvert 2,0\rangle$ | $\frac{\sqrt{2}}{\sqrt{3}}\lvert 2,+1\rangle+\frac{1}{\sqrt{3}}\lvert 2,-2\rangle$ |
| | $\lvert E,\epsilon\rangle$ | $\frac{1}{\sqrt{2}}\lvert 2,+2\rangle+\frac{1}{\sqrt{2}}\lvert 2,-2\rangle$ | $-\frac{1}{\sqrt{3}}\lvert 2,+2\rangle+\frac{\sqrt{2}}{\sqrt{3}}\lvert 2,-1\rangle$ |
| | $\lvert T_2,+1'\rangle$ | $\lvert 2,-1\rangle$ | $-\frac{1}{\sqrt{3}}\lvert 2,+1\rangle+\frac{\sqrt{2}}{\sqrt{3}}\lvert 2,-2\rangle$ |
| | $\lvert T_2,0'\rangle$ | $\frac{1}{\sqrt{2}}\lvert 2,+2\rangle-\frac{1}{\sqrt{2}}\lvert 2,-2\rangle$ | $\lvert 2,0\rangle$ |
| | $\lvert T_2,-1'\rangle$ | $-\lvert 2,+1\rangle$ | $-\frac{\sqrt{2}}{\sqrt{3}}\lvert 2,+2\rangle-\frac{1}{\sqrt{3}}\lvert 2,-1\rangle$ |

TABLE V. Normalized coupling coefficients $\langle E_{5/2}\gamma,\Gamma'\gamma'\lvert G_{3/2}\gamma''\rangle$ for the cubic point group $O$ taking (a) the [001] axis and (b) the [111] axis as the quantization axis.

(a) $\hat{z}\parallel[001]$

| $E_{5/2}\times E$ | | $G_{3/2}$ $(J=\frac{3}{2},\frac{5}{2},\frac{7}{2})$ | | | |
|---|---|---|---|---|---|
| | | $\kappa$ | $\lambda$ | $\mu$ | $\nu$ |
| $\alpha''$ | $\theta$ | | | | $-1$ |
| $\alpha''$ | $\epsilon$ | | 1 | | |
| $\beta''$ | $\theta$ | 1 | | | |
| $\beta''$ | $\epsilon$ | | | $-1$ | |

| $E_{5/2}\times T_1$ | | $G_{3/2}$ $(J=\frac{3}{2},\frac{5}{2},\frac{7}{2})$ | | | | $E_{5/2}\times T_2$ | | $G_{3/2}$ $(J=\frac{3}{2},\frac{5}{2},\frac{7}{2})$ | | | |
|---|---|---|---|---|---|---|---|---|---|---|---|
| | | $\kappa$ | $\lambda$ | $\mu$ | $\nu$ | | | $\kappa$ | $\lambda$ | $\mu$ | $\nu$ |
| $\alpha''$ | $+1$ | | | $-1$ | | $\alpha''$ | $+1'$ | 1 | | | |
| $\alpha''$ | 0 | | | | $\frac{\sqrt{2}}{\sqrt{3}}$ | $\alpha''$ | $0'$ | | $\frac{\sqrt{2}}{\sqrt{3}}$ | | |
| $\alpha''$ | $-1$ | $\frac{1}{\sqrt{3}}$ | | | | $\alpha''$ | $-1'$ | | | $\frac{1}{\sqrt{3}}$ | |
| $\beta''$ | $+1$ | | | | $\frac{1}{\sqrt{3}}$ | $\beta''$ | $+1'$ | | $\frac{1}{\sqrt{3}}$ | | |
| $\beta''$ | 0 | $\frac{\sqrt{2}}{\sqrt{3}}$ | | | | $\beta''$ | $0'$ | | | $\frac{\sqrt{2}}{\sqrt{3}}$ | |
| $\beta''$ | $-1$ | | $-1$ | | | $\beta''$ | $-1'$ | | | | 1 |

(b) $\hat{z}\parallel[111]$

| $E_{5/2}\times E$ | | $G_{3/2}$ $(J=\frac{3}{2})$ | | | | $G_{3/2}$ $(J=\frac{5}{2})$ | | | | $G_{3/2}$ $(J=\frac{7}{2})$ | | | |
|---|---|---|---|---|---|---|---|---|---|---|---|---|---|
| | | $\kappa_{3/2}$ | $\lambda_{3/2}$ | $\mu_{3/2}$ | $\nu_{3/2}$ | $\kappa_{5/2}$ | $\lambda_{5/2}$ | $\mu_{5/2}$ | $\nu_{5/2}$ | $\kappa_{7/2}$ | $\lambda_{7/2}$ | $\mu_{7/2}$ | $\nu_{7/2}$ |
| $\alpha''$ | $\theta$ | $-\frac{1}{\sqrt{3}}$ | | | $-\frac{\sqrt{2}}{\sqrt{3}}$ | $-\frac{1}{3}$ | | | $-\frac{2\sqrt{2}}{3}$ | $\frac{1}{3}$ | | | $-\frac{2\sqrt{2}}{3}$ |
| $\alpha''$ | $\epsilon$ | | | 1 | | | | 1 | | | | 1 | |
| $\beta''$ | $\theta$ | | 1 | | | | 1 | | | | 1 | | |
| $\beta''$ | $\epsilon$ | $\frac{\sqrt{2}}{\sqrt{3}}$ | | | $-\frac{1}{\sqrt{3}}$ | $\frac{2\sqrt{2}}{3}$ | | | $-\frac{1}{3}$ | $\frac{2\sqrt{2}}{3}$ | | | $\frac{1}{3}$ |

TABLE V. (*Continued*).

| $E_{5/2}\times T_1$ | | $G_{3/2}$ $(J=\frac{3}{2})$ | | | | $G_{3/2}$ $(J=\frac{5}{2})$ | | | | $G_{3/2}$ $(J=\frac{7}{2})$ | | | |
|---|---|---|---|---|---|---|---|---|---|---|---|---|---|
| | | $\kappa_{3/2}$ | $\lambda_{3/2}$ | $\mu_{3/2}$ | $\nu_{3/2}$ | $\kappa_{5/2}$ | $\lambda_{5/2}$ | $\mu_{5/2}$ | $\nu_{5/2}$ | $\kappa_{7/2}$ | $\lambda_{7/2}$ | $\mu_{7/2}$ | $\nu_{7/2}$ |
| $\alpha''$ | $+1$ | $-\frac{1}{3}$ | | | $\frac{2\sqrt{2}}{3}$ | $-\frac{1}{\sqrt{3}}$ | | | $\frac{\sqrt{2}}{\sqrt{3}}$ | $-\frac{5}{3\sqrt{3}}$ | | | $\frac{\sqrt{2}}{3\sqrt{3}}$ |
| $\alpha''$ | 0 | | $\frac{\sqrt{2}}{\sqrt{3}}$ | | | | $\frac{\sqrt{2}}{\sqrt{3}}$ | | | | $\frac{\sqrt{2}}{\sqrt{3}}$ | | |
| $\alpha''$ | $-1$ | | | $-\frac{1}{\sqrt{3}}$ | | | | $-\frac{1}{\sqrt{3}}$ | | | | $-\frac{1}{\sqrt{3}}$ | |
| $\beta''$ | $+1$ | | $\frac{1}{\sqrt{3}}$ | | | | $\frac{1}{\sqrt{3}}$ | | | | $\frac{1}{\sqrt{3}}$ | | |
| $\beta''$ | 0 | | | $-\frac{\sqrt{2}}{\sqrt{3}}$ | | | | $-\frac{\sqrt{2}}{\sqrt{3}}$ | | | | $-\frac{\sqrt{2}}{\sqrt{3}}$ | |
| $\beta''$ | $-1$ | $\frac{2\sqrt{2}}{3}$ | | | $\frac{1}{3}$ | $\frac{\sqrt{2}}{\sqrt{3}}$ | | | $\frac{1}{\sqrt{3}}$ | $\frac{\sqrt{2}}{3\sqrt{3}}$ | | | $\frac{5}{3\sqrt{3}}$ |

| $E_{5/2}\times T_2$ | | $G_{3/2}$ $(J=\frac{3}{2})$ | | | | $G_{3/2}$ $(J=\frac{5}{2})$ | | | | $G_{3/2}$ $(J=\frac{7}{2})$ | | | |
|---|---|---|---|---|---|---|---|---|---|---|---|---|---|
| | | $\kappa_{3/2}$ | $\lambda_{3/2}$ | $\mu_{3/2}$ | $\nu_{3/2}$ | $\kappa_{5/2}$ | $\lambda_{5/2}$ | $\mu_{5/2}$ | $\nu_{5/2}$ | $\kappa_{7/2}$ | $\lambda_{7/2}$ | $\mu_{7/2}$ | $\nu_{7/2}$ |
| $\alpha''$ | $+1'$ | 1 | | | | $\frac{5}{3\sqrt{3}}$ | | | $\frac{\sqrt{2}}{3\sqrt{3}}$ | $\frac{1}{\sqrt{3}}$ | | | $\frac{\sqrt{2}}{\sqrt{3}}$ |
| $\alpha''$ | $0'$ | | $\frac{\sqrt{2}}{\sqrt{3}}$ | | | | $\frac{\sqrt{2}}{\sqrt{3}}$ | | | | $\frac{\sqrt{2}}{\sqrt{3}}$ | | |
| $\alpha''$ | $-1'$ | | | $\frac{1}{\sqrt{3}}$ | | | | $\frac{1}{\sqrt{3}}$ | | | | $\frac{1}{\sqrt{3}}$ | |
| $\beta''$ | $+1'$ | | $\frac{1}{\sqrt{3}}$ | | | | $\frac{1}{\sqrt{3}}$ | | | | $\frac{1}{\sqrt{3}}$ | | |
| $\beta''$ | $0'$ | | | $\frac{\sqrt{2}}{\sqrt{3}}$ | | | | $\frac{\sqrt{2}}{\sqrt{3}}$ | | | | $\frac{\sqrt{2}}{\sqrt{3}}$ | |
| $\beta''$ | $-1'$ | | | | 1 | $-\frac{\sqrt{2}}{3\sqrt{3}}$ | | | $\frac{5}{3\sqrt{3}}$ | $-\frac{\sqrt{2}}{\sqrt{3}}$ | | | $\frac{1}{\sqrt{3}}$ |

pling coefficients by using the eigenfunctions and the Clebsch-Gordon coefficients.

We consider the states with $J=\frac{3}{2}$, $\frac{5}{2}$, and $\frac{7}{2}$ of a Kramers ion in a cubic field, so that the electronic states are characterized by the irreducible representations $E_{1/2}$, $E_{5/2}$, and $G_{3/2}$ of the double group. The crystalline-field Hamiltonian in a cubic field is expressed in the standard notation[22] as

$$\mathcal{H}_c=\begin{cases} B_4(O_4^0+5O_4^4)+B_6(O_6^0-21O_6^4), & \hat{\mathbf{z}}\|[001]\,, \qquad \text{(A1)} \\ -\frac{2}{3}B_4(O_4^0+20\sqrt{2}O_4^3)+\frac{16}{9}B_6\left[O_6^0-\frac{35\sqrt{2}}{4}O_6^3+\frac{77}{8}O_6^6\right], & \hat{\mathbf{z}}\|[111]. \qquad \text{(A2)} \end{cases}$$

The first form (A1) is referred to the fourfold axes ($\hat{\mathbf{z}}\|[001]$) and the second form (A2) to the threefold axes ($\hat{\mathbf{z}}\|[111]$). The energy eigenvalues and eigenfunctions for the Hamiltonian are obtained from the known matrix elements of the crystalline-field operators.[23] The obtained eigenfunctions are listed in Table I. They are also the eigenfunctions in the magnetic field along each axis ($\mathbf{H}\|\hat{\mathbf{z}}$) as long as the field is not too strong.

The selection rules between $\Gamma$ and $\Gamma''$ states for $\Gamma'$ symmetry of the transition can be obtained by reducing $\Gamma\times\Gamma'$ in terms of $\Gamma''$, where $\Gamma$, $\Gamma'$, and $\Gamma''$ are the irreducible representations of the group. The relative transition probabilities are obtained from the squares of the coupling coefficients. The coupling coefficients $\langle\Gamma(J)\gamma,\Gamma'(J')\gamma'|\Gamma''(J'')\gamma''\rangle$ are defined by the coefficients in the expansion

$$|\Gamma''(J''),\gamma''\rangle=\sum_{\gamma}\sum_{\gamma'}|\Gamma(J)\gamma,\Gamma'(J')\gamma'\rangle\langle\Gamma(J)\gamma,\Gamma'(J')\gamma'|\Gamma''(J'')\gamma''\rangle\,, \qquad \text{(A3)}$$

where $|\Gamma(J)\gamma,\Gamma'(J')\gamma'\rangle=|\Gamma(J),\gamma\rangle|\Gamma'(J'),\gamma'\rangle$ and $|\Gamma(J),\gamma\rangle$ represents one of the eigenfunctions (bases) for the irreducible representation $\Gamma$ labeled by $J$.

The expression of the coupling coefficients is derived as follows. As shown in Table I the eigenfunctions in the crystalline field are given by linear combinations of the eigenfunctions $|J,M\rangle$ of a free ion:

$$|\Gamma(J),\gamma\rangle=\sum_M a(\Gamma\gamma JM)|J,M\rangle \ . \tag{A4}$$

Therefore, we can calculate the coupling coefficients from the Clebsch-Gordon coefficients $\langle JM,J'M'|J''M''\rangle$ defined by

$$|J'',M''\rangle=\sum_M\sum_{M'}|JM,J'M'\rangle\langle JM,J'M'|J''M''\rangle \ , \tag{A5}$$

where $|JM,J'M'\rangle=|J,M\rangle|J',M'\rangle$. From Eqs. (A3)–(A5) we obtain the expression of the coupling coefficients

$$\langle\Gamma(J)\gamma,\Gamma'(J')\gamma'|\Gamma''(J'')\gamma''\rangle=\left\{\sum_M\sum_{M'}a^*(\Gamma\gamma JM)a'^*(\Gamma'\gamma'J'M')\langle JM,J'M'|\right\}\left\{\sum_{M''}a''(\Gamma''\gamma''J''M'')|J'',M''\rangle\right\}$$
$$=\sum_M\sum_{M'}\sum_{M''}a^*(\Gamma\gamma JM)a'^*(\Gamma'\gamma'J'M')a''(\Gamma''\gamma''J''M'')\langle JM,J'M'|J''M''\rangle \ . \tag{A6}$$

This expression is quite general and not restricted to the cubic point group $O$.

We are interested in the transition between $\Gamma=E_{5/2}$ and $\Gamma''=G_{3/2}$ states for $J=\frac{3}{2}$, $\frac{5}{2}$, and $\frac{7}{2}$ as discussed in Secs. II and III. Three symmetries $\Gamma'=E$, $T_1$, and $T_2$ are allowed for the transition ($E_{5/2}\times G_{3/2}=E+T_1+T_2$). For the symmetries of the transitions we use the irreducible representations $E$ ($J=2$), $T_1$ ($J=1$), and $T_2$ ($J=2$). Their bases are also derived from Eqs. (A1) and (A2), and are shown in Table IV. Table V shows the calculated values of the coupling coefficients derived from Eq. (A6) with Table I, Table IV, and the Clebsch-Gordan coefficients.[24] The selection rules and the relative transition probabilities used to calculate the spin polarization in Table III are obtained from the coupling coefficients in Table V.

As shown in Table V the coupling coefficients generally depend on the quantization axis and the $J$ value. However, those for $\hat{\mathbf{z}}\|[001]$ do not depend on the $J$ value ($J=\frac{5}{2}$ and $\frac{7}{2}$ for $E_{5/2}$, $J=\frac{3}{2}$, $\frac{5}{2}$, and $\frac{7}{2}$ for $G_{3/2}$). The eigenfunctions and coupling coefficients given in standard textbooks[14,15] are those for $\hat{\mathbf{z}}\|[001]$.

In the derivation of Table V we used the bases of the irreducible representations shown in Table IV for the symmetries of the transitions. The coupling coefficients in Table V are changed if we use the bases of the irreducible representations labeled by different values of $J$ such as $E$ ($J=4$), $T_1$ ($J=3$), and $T_2$ ($J=3$). But, as shown in the following, the spin-memory effect does not depend on the $J$ value of the transition symmetry, as long as the decay is a spontaneous process. The transition probability between $|\Gamma,\gamma\rangle$ and $|\Gamma'',\gamma''\rangle$ states for the transition of $\Gamma'$ symmetry is proportional to the quantity

$$\sum_{\gamma'}|\langle\Gamma\gamma,\Gamma'\gamma'|\Gamma''\gamma''\rangle|^2 \ , \tag{A7}$$

when the transition is a spontaneous process. We consider two irreducible representations $\Gamma'(J_1)$ and $\Gamma'(J_2)$ for the symmetry of the transition ($J_1\neq J_2$), whose bases are written by $\delta$ and $\rho$. One set of the bases can be represented by the linear combinations of the other set. From the definition of the coupling coefficient in Eq. (A3) and the orthogonal character of the coefficients in the linear combinations, we can show the following relation:

$$\sum_\delta|\langle\Gamma\gamma,\Gamma'\delta|\Gamma''\gamma''\rangle|^2=\sum_\rho|\langle\Gamma\gamma,\Gamma'\rho|\Gamma''\gamma''\rangle|^2 \ . \tag{A8}$$

Therefore, the transition probability does not depend on the $J$ value of $\Gamma'$ for the spontaneous process. The decay from the band to the metastable state discussed in this paper is characterized only by the symmetry, and that the spin-memory effect does not depend on the $J$ value of the transition symmetry. The bases for the specific $J$ values in Table IV are sufficient to derive the spin polarization in Table III.


[1] T. Kohmoto, Y. Fukuda, and T. Hashi, Phys. Rev. B **34**, 6085 (1986).

[2] G. F. Imbusch and S. Geschwind, Phys. Rev. Lett. **17**, 238 (1966).

[3] P. Kisliuk, H. H. Tippins, C. A. Moore, and S. A. Pollack, Phys. Rev. **171**, 336 (1968).

[4] D. H. Tanimoto, W. M. Ziniker, and J. O. Kemp, Phys. Rev. Lett. **14**, 645 (1965).

[5] L. F. Mollenauer, S. Pan, and S. Yngvesson, Phys. Rev. Lett. **23**, 683 (1969).

[6] H. Ohkura, K. Iwahana, M. Tanaka, K. Tara, and K. Imanaka, J. Phys. Soc. Jpn. **49**, 2296 (1980).

[7] G. Baldacchini, G. P. Gallerano, U. M. Grassano, and F. Luty, Phys. Rev. B **27**, 5039 (1983).

[8] C. H. Anderson, H. A. Weakliem, and E. S. Sabisky, Phys. Rev. **143**, 223 (1966).

[9] H. A. Weakliem, C. H. Anderson, and E. S. Sabisky, Phys. Rev. B **2**, 4354 (1970).

[10] Y. R. Shen, Phys. Rev. **134**, A661 (1964).

[11] C. H. Anderson and E. S. Sabisky, Phys. Rev. **178**, 547 (1969).

[12]T. Kohmoto, Y. Fukuda, and T. Hashi, Phys. Rev. B **34**, 6094 (1986).
[13]J. S. Griffith, *The Theory of Transition-Metal Ions* (Cambridge University Press, England, 1964), Appendix 2, Table A14.
[14]Griffith (Ref. 13), Appendix 2, Tables A19 and A20.
[15]A. Abragam and B. Bleaney, *Electron Paramagnetic Resonance of Transition Ions* (Clarendon, Oxford, 1970), Appendix B, Table 9.
[16]K. R. Lea, M. J. M. Leask, and W. P. Wolf, J. Phys. Chem. Solids **23**, 1381 (1962).
[17]C. H. Anderson and E. S. Sabisky, in *Physical Acoustics*, edited by W. P. Mason and R. N. Thurston (Academic, New York, 1971), Vol. VIII, p. 21.
[18]L. A. Riseberg and H. W. Moos, Phys. Rev. **174**, 429 (1968).
[19]M. J. Weber, Phys. Rev. B **8**, 54 (1973).
[20]Z. J. Kiss, Phys. Rev. **127**, 718 (1962).
[21]W. B. Grant, L. F. Mollenauer, and C. D. Jeffries, Phys. Rev. B **4**, 1428 (1971).
[22]J. M. Baker, B. Bleaney, and W. Hayes, Proc. R. Soc. London Ser. **A247**, 141 (1958).
[23]Abragam and Bleaney (Ref. 15), Appendix B, Table 17.
[24]T. Inoue, *Table of the Clebsch-Gordan Coefficients* (Tokyo Tosho Co., Tokyo, 1966).